Environmental Pollution 385 (2025) 127159

Contents lists available at ScienceDirect

Environmental Pollution

journal homepage: www.elsevier.com/locate/envpol

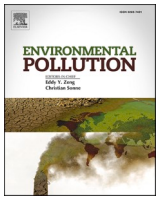

Impacts of uncertainties in Chinese NH_3 emissions on $PM_{2.5}$ concentrations over mainland China and downwind regions☆

Hyeonsik Choe [a,b], Chae-Yeong Yang [a,b], Yunsoo Choi [c], Jincheol Park [c], Dongjin Kim [a,b], Jeonghyeok Moon [d], Min Heo [a,b], Jaehyeong Park [a], Cheol-Hee Kim [b,e,f], Wonbae Jeon [b,f,*]

[a] Division of Earth Environmental System, Pusan National University, Busan, 46241, South Korea
[b] BK21 School of Earth and Environmental System, Pusan National University, Busan, 46241, South Korea
[c] Department of Earth and Atmospheric Sciences, University of Houston, Houston, TX, USA
[d] Environmental Planning Institute, Seoul National University, Seoul, 08826, South Korea
[e] Institute of Environmental Studies, Pusan National University, Busan, 46241, South Korea
[f] Department of Atmospheric Sciences, Pusan National University, Busan, 46241, South Korea

ARTICLE INFO

Keywords:
CMAQ
Ammonia
Emission
$PM_{2.5}$
Transboundary transport

ABSTRACT

Uncertainties in ammonia (NH_3) emissions can influence ambient fine particulate matter ($PM_{2.5}$) concentrations through atmospheric chemical reactions. In this study, we performed numerical simulations using the Community Multiscale Air Quality (CMAQ) model to assess how uncertainties in Chinese NH_3 emissions affect $PM_{2.5}$ concentrations over mainland China and its downwind regions. We designed perturbation scenarios for spring and summer 2019 by increasing NH_3 emissions by 75.7 %, reflecting values reported in previous studies. Although the emission increase was larger in summer (2.00 mol/s) than in spring (1.05 mol/s), $PM_{2.5}$ concentration changes were more pronounced in spring (2.54 μg/m^3) than in summer (1.99 μg/m^3). The greater $PM_{2.5}$ response in spring is attributed to the nitrate (NO_3^-) production–loss mechanism ($NH_3 + HNO_3 \rightleftharpoons NH_4^+ + NO_3^-$). Despite the larger increase in NH_3 emissions during summer, the net rise in NO_3^- was lower than in spring because the dominant NO_3^- decomposition rate of −1.229 μg/m^3/h under higher temperatures offset production. Concurrently, seasonal shifts in synoptic wind patterns were found to significantly modulate downwind $PM_{2.5}$ concentration variations attributable to emission heterogeneity. Springtime atmospheric circulation facilitated efficient transboundary transport of NO_3^- towards the Korean Peninsula, consequently elevating $PM_{2.5}$ concentrations in downwind Seoul by 3.07 μg/m^3, surpassing the 2.75 μg/m^3 increase observed in upwind Beijing. In stark contrast, summertime circulation impeded NO_3^- advection, resulting in a mere 0.15 μg/m^3 $PM_{2.5}$ change in Seoul compared to 2.42 μg/m^3 in Beijing. These findings underscore that variations in NH_3 emissions from China can profoundly influence regional $PM_{2.5}$ levels, and that meteorological conditions, particularly wind patterns, play a pivotal role in dictating East Asian air quality.

1. Introduction

Fine particulate matter ($PM_{2.5}$) can adversely affect human health by increasing the risk of respiratory and cardiovascular diseases (Liu et al., 2018; Pun et al., 2017; Jeon et al., 2015; Erisman & Schaap, 2004). $PM_{2.5}$ consists of various chemical components, and the relative contribution of each component varies with regional characteristics and seasonal meteorological conditions (Cheng et al., 2016; Bell et al., 2007; Ye et al., 2003). In East Asia, secondary inorganic aerosols such as particulate sulfate (SO_4^{2-}), nitrate (NO_3^-), and ammonium (NH_4^+) account for a substantial fraction of $PM_{2.5}$, For example, these aerosols contributed more than 53 % of the surface $PM_{2.5}$ mass concentrations measured at six supersites across South Korea during 2019 (Park et al., 2023; Cao et al., 2017; Kai et al., 2007). Effective control of $PM_{2.5}$ concentrations in East Asia depends on proper management of the emissions of $PM_{2.5}$ precursor species, particularly sulfur oxides (SO_x), nitrogen oxides (NO_x), and ammonia (NH_3). Recent scenario-based studies also demonstrated that large-scale electrification of vehicles in China could substantially reduce $PM_{2.5}$ and NO_2 concentrations, highlighting the importance of policy-driven emission reductions for

☆ This paper has been recommended for acceptance by Prof. Pavlos Kassomenos.

* Corresponding author. Department of Atmospheric Sciences, Pusan National University, Busandaehak-ro 63beon-gil, Geumjeong-gu, Busan, 46241, South Korea.
E-mail address: wbjeon@pusan.ac.kr (W. Jeon).

https://doi.org/10.1016/j.envpol.2025.127159
Received 11 July 2025; Received in revised form 7 September 2025; Accepted 22 September 2025
Available online 25 September 2025

improving air quality in the region (Wang et al., 2021a). Consistent with these insights, historical emission trends reveal that from 2000 to 2018, NO_x and SO_x emissions in China declined due to sustained regulatory efforts, whereas NH_3 emissions received comparatively little policy attention and increased significantly during the same period (Chen et al., 2023; Crippa et al., 2023; Liu et al., 2020; Zheng et al., 2018), underscoring its growing role in East Asia's atmospheric chemistry.

Gas-phase air pollutants originating in China undergo chemical transformation during long-range transport, often affecting air quality in neighboring regions, and in East Asia, seasonal atmospheric circulation strongly modulates the influx of $PM_{2.5}$ precursors to South Korea (Jeon et al., 2021; Bae et al., 2019; Kim et al., 2017a; Oh et al., 2015; Kaneyasu et al., 2014). For example, Kim et al. (2017b) revealed that the contribution of foreign transboundary emissions to $PM_{2.5}$ concentrations in the Seoul metropolitan area (SMA) was approximately 45 % in summer and increased to over 70 % in spring 2014. More recently, Park et al. (2025) reported that the contribution of reactive nitrogen (NO_y) transported from China to South Korea increased from 27 to 32 % in winter to 34–37 % in spring 2022.

Despite the widely acknowledged contribution of China's pollutant emissions to shaping aerosol loadings across East Asia, the specific role of NH_3 remains comparatively underexplored. Understanding the impact of NH_3 emissions from China on $PM_{2.5}$ formation is critical not only for local air quality management but also for informing neighboring countries' responses to transboundary pollution. However, bottom-up estimates of NH_3 emissions from China still remain subject to substantial uncertainties (Chen et al., 2023; Huang et al., 2012; Dong et al., 2010), which may compromise the reliability of chemical transport model (CTM) simulations, leading to difficulty in accurately attributing the contributions of emission sources to $PM_{2.5}$ loadings across East Asia. While several studies have investigated the implications of uncertainties in NH_3 emissions within China (Momeni et al., 2024; Wang et al., 2024), relatively few have assessed their influence on air quality in downwind regions. Recent observational studies in East Asia, including Nirmalkar et al. (2023) and Nirmalkar et al. (2021), have highlighted the importance of secondary aerosol formation and regional transport during haze episodes. However, these studies mainly focused on chemical characterization and transport processes, without directly addressing the uncertainty of NH_3 emissions. In contrast, our study explicitly evaluates how such uncertainties in China influence downwind $PM_{2.5}$ concentrations in South Korea through scenario-based CMAQ simulations and process analysis.

To better understand the contribution of China's NH_3 emissions to downwind $PM_{2.5}$ concentrations across East Asia, particularly focusing on South Korea, we examined the responses of modeled $PM_{2.5}$ concentrations during spring and summer 2019 under two emissions scenarios using the Community Multiscale Air Quality (CMAQ) model (Appel et al., 2021; Ching & Byun, 1999). The baseline scenario employed the NH_3 emissions inventoried in the Emissions Database for Global Atmospheric Research (EDGAR), and the alternative scenario applied the emissions adjusted according to Liu et al. (2022), representing one of the estimates suggested in recent literature. After comprehensive model evaluation using satellite-based columnar measurements of NH_3 abundances and ground-based station measurements of $PM_{2.5}$ concentrations, we conducted a series of diagnostic analyses based on the alternative scenario. In particular, we performed the Integrated Process Rate (IPR) analysis to quantify the formation and removal rates of NO_3^- aerosols in response to the increase in NH_3 emissions, with contrasting chemical responses over inland regions and adjacent open water. This allowed us to identify the specific atmospheric processes contributing to changes in $PM_{2.5}$ concentrations in downwind areas.

2. Materials and methods

2.1. Modeling system

We conducted air quality simulations using a one-way offline Weather Research and Forecasting (WRF) and CMAQ modeling system, in which meteorological fields generated by the WRF model were used to drive the Community Multiscale Air Quality (CMAQ) model for simulating atmospheric chemistry and transport. The simulations employed WRF version 4.1.1 (Skamarock et al., 2019) and CMAQ version 5.3.2, a widely used chemical transport model (CTM) that represents the three-dimensional formation, transformation, and transport of air pollutants using modeled meteorological fields and prescribed emissions.

For regional-scale modeling over East Asia, we configured a 15 km resolution domain (D01) encompassing eastern China, the Bohai Sea, and the Korean Peninsula (Fig. 1). To reduce uncertainties associated with a single nested domain, particularly those related to lateral boundary conditions, we used initial and boundary conditions obtained from hemispheric CMAQ simulations conducted by the U.S. EPA (U.S. Environmental Protection Agency, 2018). These externally generated fields improved the accuracy of regional simulations by providing chemically consistent inflow across domain boundaries (Appel et al., 2021; Mathur et al., 2017). Gas-phase and aerosol processes were represented using the Carbon Bond 6 chemical mechanism with chlorine chemistry (CB6r3) (Emery et al., 2015) and the seventh-generation CMAQ aerosol module (AERO7). Initial and boundary conditions for the WRF simulations were derived from ERA5, the fifth-generation reanalysis from the European Centre for Medium-Range Weather Forecasts (ECMWF) (Hersbach et al., 2020), and grid nudging was applied to further constrain the meteorological fields (Souri et al., 2017).

Given the pronounced seasonal variability in NH_3 emissions and their influence on $PM_{2.5}$ concentrations (Kharol et al., 2013), we selected spring and summer to assess how emission differences and atmospheric circulation patterns affect $PM_{2.5}$ concentrations in China and downwind regions, including the Korean Peninsula. Our analysis focused on March 1–31 for spring and June 1–30 for summer. Detailed configurations used for the CMAQ and WRF simulations are provided in Tables S1 and S2.

2.2. Emissions

To prepare comprehensive emissions input for CMAQ, we combined anthropogenic and biogenic emissions of key precursor gases and primary aerosols. Anthropogenic emissions were derived from the Hemispheric Transport of Air Pollution version 3 (HTAPv3) mosaic emissions inventory provided by EDGAR. The EDGAR-HTAP v3 inventory is a mosaic dataset that integrates multiple regional inventories. For East Asia, it uses the Regional Emission inventory in Asia (REAS) for China and the Clean Air Policy Support System (CAPSS) for South Korea (Choi et al., 2022; Kurokawa and Ohara, 2019). The HTAPv3 mosaic inventory provides global monthly and annual emissions of major air pollutants including NO_x, SO_2, and NH_3 on a $0.1^\circ \times 0.1^\circ$ grid, which we regirded to a 15 km horizontal resolution for this study (Crippa et al., 2023). Then, we prepared biogenic emissions using the Model of Emissions of Gases and Aerosols from Nature (MEGAN) version 2.1 (Guenther et al., 2012). MEGAN generates emissions of biogenic VOCs and other trace gases based on vegetative surface properties, emission factors, and their responsiveness to WRF-simulated meteorological conditions. This ensures that the emissions retain spatial consistency with WRF outputs, allowing direct integration into CMAQ. We merged these anthropogenic and biogenic emissions to prepare CMAQ-ready emissions input for our simulations for 2019. The emission data processed for the model simulations did not include natural sources such as sea salt, biomass burning, and dust.

Fig. 2 compares monthly mean NO_x, SO_2, and NH_3 emissions across

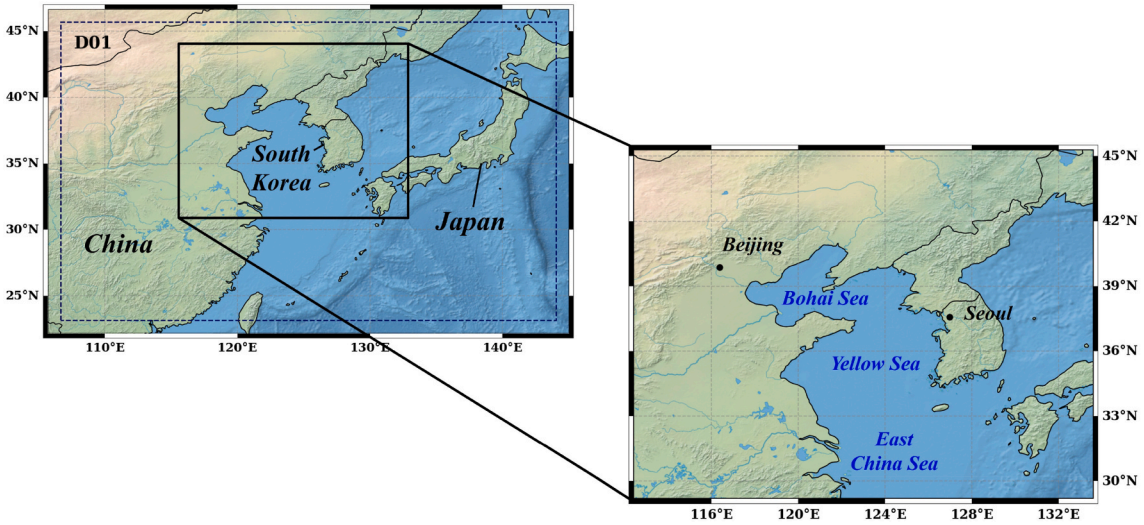

Fig. 1. Modeling domain (D01) for WRF and CMAQ simulations over East Asia. The left shows the full domain including China, Korea, Japan, and surrounding seas. The right panel provides an enlarged view of eastern China and the Korean Peninsula, indicating key geographical features such as the Bohai Sea, Yellow Sea, and major cities (e.g., Beijing and Seoul). (For interpretation of the references to colour in this figure legend, the reader is referred to the Web version of this article.)

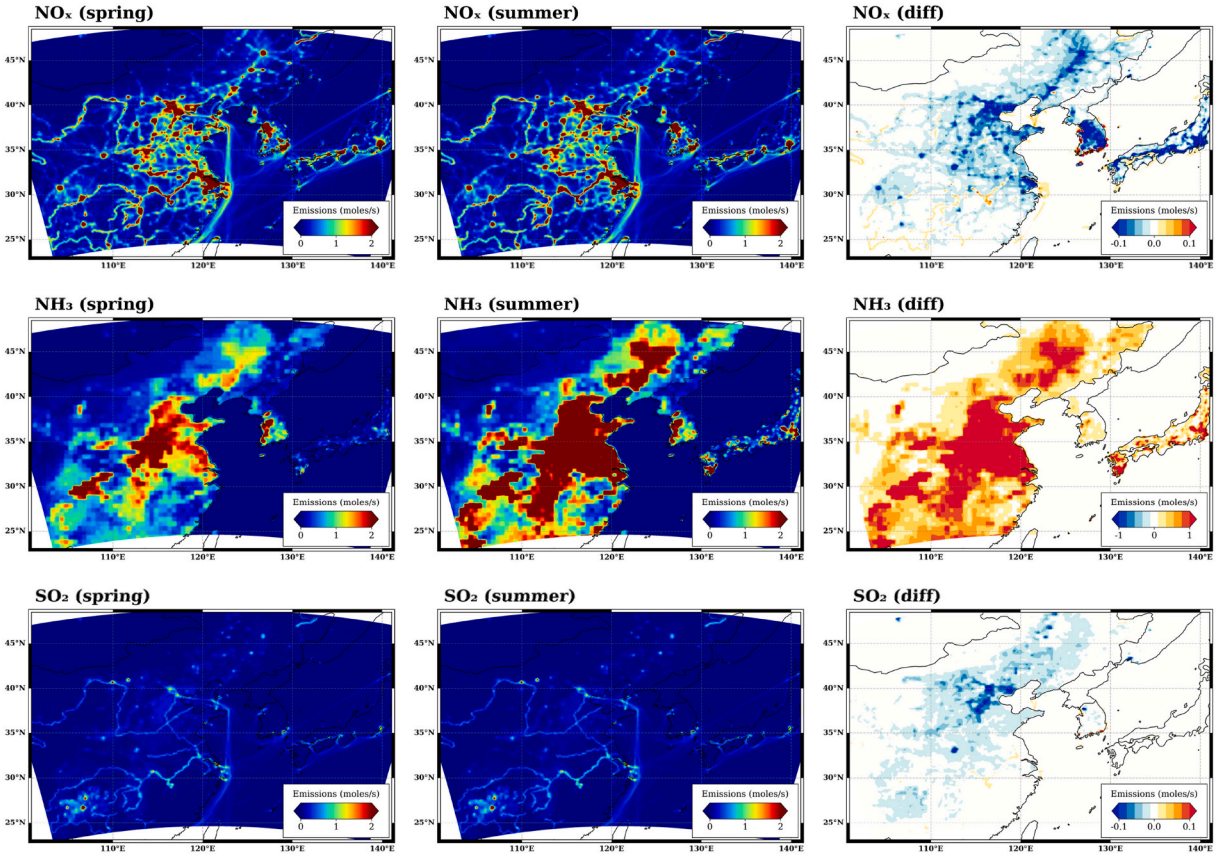

Fig. 2. Spatial distributions of averaged anthropogenic NO_x, NH_3, and SO_2 emissions (moles/s) across East Asia for spring (March), summer (June) and their diff (summer – spring). Emission rates are based on the HTAP v3 inventory and are expressed in moles per second, illustrating seasonal and spatial variability over the simulation domain.

East Asia for March (spring) and June (summer). NO_x and SO_2 emissions remain focused in urban and industrial areas and along major shipping lanes, exhibiting relatively minor seasonal variations. Whereas NH_3 emissions differ by more than 1 mol/s between spring and summer, with emissions largely confined to intensive agricultural hotspots in spring, but spreading extensively over croplands of the North China Plain in summer. In this study, the analysis periods were set to spring and summer to investigate changes in $PM_{2.5}$ concentrations over China and downwind regions resulting from variations in NH_3 emissions. In spring, NH_3 emissions are relatively low, but prevailing easterly winds efficiently transport pollutants from China to downwind areas, potentially amplifying the effects of emission changes. In contrast, summer features

the highest NH_3 emissions of the four seasons, so that a uniform proportional increase in emissions produces the largest absolute increase.

2.3. Experimental design

We conducted two CMAQ simulations to assess the influence of uncertainties in China's NH_3 emissions on $PM_{2.5}$ concentrations across East Asia. The baseline (BASE) case used the emissions prepared in Section 2.2, while in the experimental (HIGH) case, China's NH_3 emissions were scaled up by 75.7 %. This scaling factor was derived from Liu et al. (2022), who showed using IASI and GIIRS satellite observations that conventional inventories such as EDGAR substantially underestimate Chinese NH_3 emissions, with discrepancies reaching up to 75.7 %. Based on this evidence, the HIGH case was designed to evaluate the impact of such underestimation on simulated $PM_{2.5}$ components. The abundance of NH_3 directly influences the concentrations of secondary inorganic aerosols such as NO_3^-, SO_4^{2-}, and NH_4^+ (Liang et al., 2024; Kai et al., 2007), which collectively account for a substantial fraction of total $PM_{2.5}$ mass concentrations. Accordingly, we performed IPR analysis to investigate the production and removal mechanisms of $PM_{2.5}$ components, building on previous aerosol studies focused on East Asia (Li et al., 2014). The IPR is CMAQ's built-in diagnostic tool that quantifies the net contributions of individual processes, such as horizontal and vertical transport, dry deposition, and aerosol processes (AERO), to changes in pollutant concentrations over time. In particular, the AERO output characterizes the partitioning dynamics between gas-phase precursors and particle-phase constituents of secondary aerosols (Shen et al., 2020; Liu et al., 2010). To clarify, a positive contribution reflects gas-to-aerosol formation, whereas a negative contribution indicates partitioning in the reverse direction (Park et al., 2022; Qu et al., 2021). This allowed us to attribute changes in $PM_{2.5}$ concentrations to specific physicochemical processes, with particular emphasis on AERO-driven NO_3^- partitioning across seasons and regions. In CMAQ, the AERO process is calculated using the ISORROPIA II thermodynamic equilibrium module, which determines gas–particle partitioning of semi-volatile inorganic species such as NH_4NO_3 depending on temperature, relative humidity, and precursor concentrations (Nirmalkar et al., 2023; Fountoukis and Nenes, 2007).

2.4. Surface and satellite measurements

We evaluated the accuracy of our baseline simulations using ground-based station measurements and satellite observation data. For WRF-simulated near-surface meteorological fields, we used surface meteorological variables measured at 95 sites in South Korea and 350 sites in China, provided by the Korea Meteorological Administration's Automated Synoptic Observing System and the Global Telecommunication System, respectively. For CMAQ-simulated surface $PM_{2.5}$ concentrations, we used hourly $PM_{2.5}$ concentrations measured at 452 Air Quality Monitoring Stations in Korea operated by the National Institute of Environmental Research (NIER) and 1451 sites in China provided by the Ministry of Ecology and Environment (MEE).

Due to the limited spatial and temporal coverage of ground-based NH_3 observations, satellite retrievals are often used for model evaluation (Liu et al., 2022; Van Damme et al., 2014; Clarisse et al., 2009). Accordingly, we used NH_3 column density data retrieved from the Infrared Atmospheric Sounding Interferometer (IASI), an infrared sensor onboard the Meteorological Operational (MetOp) satellite operated by EUMETSAT. IASI measures infrared radiation emitted by the Earth's atmosphere and provides high-resolution data on trace gases such as NH_3 and ozone (O_3) (Clarisse et al., 2023; Franco et al., 2018; Damme et al., 2017). Specifically, we used the Level 3 (L3) IASI product, which is generated by applying temporal and spatial regridding to Level 2 retrievals and is provided at a uniform grid resolution of 12 km × 12 km. This dataset is well-suited for regional and time-specific comparisons. We used the IASI L3 dataset to evaluate the model performance in simulating NH_3 concentrations and to assess the uncertainty in China's NH_3 emissions inventory.

3. Results and discussion

3.1. Evaluation of meteorological and air quality modeling performance

To evaluate the agreement between model simulations and observations, eight statistical metrics were calculated: Mean Bias (MB), Mean Error (ME), Mean Fractional Bias (MFB), Mean Fractional Error (MFE), Normalized Mean Bias (NMB), Normalized Mean Error (NME), Root Mean Square Error (RMSE), and the Correlation Coefficient (R). The definitions and formulas for these metrics are summarized in Table S3, and model performance was assessed based on the criteria proposed by Emery et al. (2017) and Boylan and Russell (2006).

Meteorological parameters strongly influence air pollution formation and transport (Sulaymon et al., 2023a; Sulaymon et al., 2023b; Ye et al., 2022; Wang et al., 2021b). To evaluate WRF performance, simulated temperature at 2 m (T2), wind speed (WS) and wind direction (WD) at 10 m, and relative humidity (RH) were compared with surface observations in China and South Korea (Tables S4–S5). In spring, T2 showed good agreement overall, with domain MB and ME of −0.8 °C and 1.5 °C. Most sites met benchmarks ($|MB| \leq 0.5$ °C), though several Korean cities showed cold biases (e.g., Busan −2.2 °C). WS was reasonably reproduced (domain MB = 0.2 m/s, ME = 1.0 m/s), despite overestimation in South Korea and slight underprediction in northern China. WD performance was weaker, MB values exceeded ±10° and ME > 30° in several Korean sites, consistent with earlier reports of large WD uncertainty. RH was underestimated in Chinese cities and overestimated in Korea, with domain MB and ME of 2.3 % and 7.3 %. These values are comparable to previous East Asian studies. In particular, model performance in South Korea was relatively poor, which can be attributed to the complex terrain and the use of a 15 km grid resolution, limiting the ability of WRF to capture local meteorological variability(Lim et al., 2019; Byon et al., 2010). Overall, WRF provided sufficiently robust meteorology to support CMAQ simulations. Detailed temporal variations of simulated and observed meteorological variables are shown in Fig. S1–S8.

The performance of CMAQ in simulating $PM_{2.5}$ was evaluated using MFB, MFE, NMB, NME, and R, with benchmarks from Boylan and Russell (2006). Table S6 summarizes results for domain averages and major cities in China and South Korea. In spring, CMAQ generally overestimated concentrations in Chinese cities, with large positive biases in Beijing (NMB = 68.2 %) and Hefei (NMB = 54.4 %), while Seoul showed slight underestimation (NMB = −10.5 %). Domain averages (MFB = 16.3 %, MFE = 36.6 %, NMB = 17.7 %, NME = 39.9 %) met benchmark criteria, and correlations were high (R = 0.73 domain-wide, >0.9 in Seoul and Gwangju). In summer, domain biases increased (NMB = 30.7 %), and correlations weakened (R = 0.66 overall, as low as 0.36 in Gwangju), though most indices remained within benchmarks. Overall, CMAQ reasonably reproduced the spatial distribution of $PM_{2.5}$ (Fig. S9), with higher concentrations over eastern China and stronger overestimation there, while showing better agreement in South Korea. These results are consistent with previous East Asian applications and provide confidence for subsequent process analyses(Hua et al., 2024; Mao et al., 2022; Wang et al., 2021b). Temporal comparisons for major cities in China and South Korea are presented in Fig. S10–S11.

Previous studies have suggested that existing emission inventories may underestimate NH_3 emissions, and such uncertainty can affect the accuracy of simulated NH_3 concentrations. Therefore, using the method detailed in Text S1 of the Supplementary, we converted CMAQ simulated NH_3 concentrations into total column values and compared them for both the BASE and HIGH cases against IASI level 3 satellite observations (Van Damme et al., 2015). In Fig. S12, the BASE case exhibited a clear tendency to underestimate NH_3, with domain-averaged NMB of 28.45 % and NME of 66.97 % in spring, and −12.18 % and 45.43 % in

summer, respectively. These results indicate that NH_3 simulations were less stable in spring, reflecting the large uncertainties in Chinese NH_3 emissions noted earlier. In the HIGH case, biases increased, but the overall regression slope and correlation improved (spring: NMB = 51.02 %, NME = 66.40 %, R = 0.69; summer: NMB = 27.32 %, NME = 53.88 %, R = 0.84). This indicates that the model more effectively captured the observed variability. Although the relatively large NME values highlight the persistent uncertainties in NH_3 emissions, the consistency of the results across seasons demonstrates that the simulations provide sufficient reliability for analyzing NH_3–$PM_{2.5}$ interactions.

3.2. Analysis of $PM_{2.5}$ concentration changes due to increased NH_3 emissions

To quantitatively assess the impact of increased NH_3 emissions on ambient $PM_{2.5}$ concentrations in East Asia, Fig. 3 presents the seasonal mean changes in NH_3 emissions and $PM_{2.5}$ concentrations averaged over the domain. As shown in Fig. 3(a), NH_3 emissions increased substantially over inland regions of China in both spring and summer, with the mean value approximately twice as high in summer (2.00 mol/s) as in spring (1.05 mol/s). In contrast, the spatial distribution of $PM_{2.5}$ concentration changes presented in Fig. 3(b) did not follow the emission pattern. The NH_3 emission increase was concentrated over inland regions, the $PM_{2.5}$ concentration increase was more pronounced over marine areas, and it was larger in spring (2.54 μg/m^3) than in summer (1.99 μg/m^3).

Although increased NH_3 emissions led to an overall rise in $PM_{2.5}$ concentrations, spatial and seasonal mismatches between emission increases and concentration responses were identified. This suggests that increased NH_3 emissions do not always directly translate into regional $PM_{2.5}$ concentration increases. Since $PM_{2.5}$ is a complex atmospheric pollutant composed of various secondary aerosol constituents such as NO_3^-, SO_4^{2-} and NH_4^+, the influence of NH_3 emission changes on the concentration of each constituent may also vary according to reactivity and transport pathways (Gong et al., 2024; Zhan et al., 2023). Therefore, we quantitatively analyzed how increased NH_3 emissions altered the concentrations of individual $PM_{2.5}$ components to identify the causes of the spatial and temporal disparities that emerged between emission changes and concentration responses.

Table S7 and Fig. S13 show the average concentration changes in $PM_{2.5}$, and its components under the HIGH case. Among the components, NO_3^- showed the largest concentration increase (1.84 μg/m^3 in spring and 1.50 μg/m^3 in summer), while NH_4^+ also exhibited significant increases in both seasons. In contrast, SO_4^{2-} showed negligible change in concentration, likely due to China's SO_2 emissions being lower than NH_3 emissions (SO_2: 8.93 Tg/yr, NH_3: 12.30 Tg/yr), as illustrated in Fig. S14. Rather than increasing SO_4^{2-}, the rise in NH_3 emissions drove NH_4NO_3 formation ($NH_3 + HNO_3 \rightleftharpoons NH_4NO_3 \rightleftharpoons NH_4^+ + NO_3^-$), raising NO_3^- and NH_4^+ concentrations because in 2018 NO_x emissions (23.59 Tg/yr) exceeded NH_3 emissions, ensuring ample HNO_3. This implies that changes in the concentrations of $PM_{2.5}$ components due to variations in NH_3 emissions are influenced by the distribution of gas-phase precursors for each aerosol component.

3.3. Spatial distribution analysis of increased NO_3^- concentrations

While increased NH_3 emissions were primarily noted over inland regions, NO_3^- concentrations rose more markedly over the ocean. This spatial discrepancy suggests that NO_3^- formation can be influenced by the spatial distribution of its precursors and atmospheric transport. In this section, we compare the spatial distributions of HNO_3 and NH_3, precursors of NO_3^-, to understand why NO_3^- concentrations increased more prominently offshore. Comparing the BASE case distributions (Fig. S15), NH_3 concentrations are highest inland, whereas HNO_3

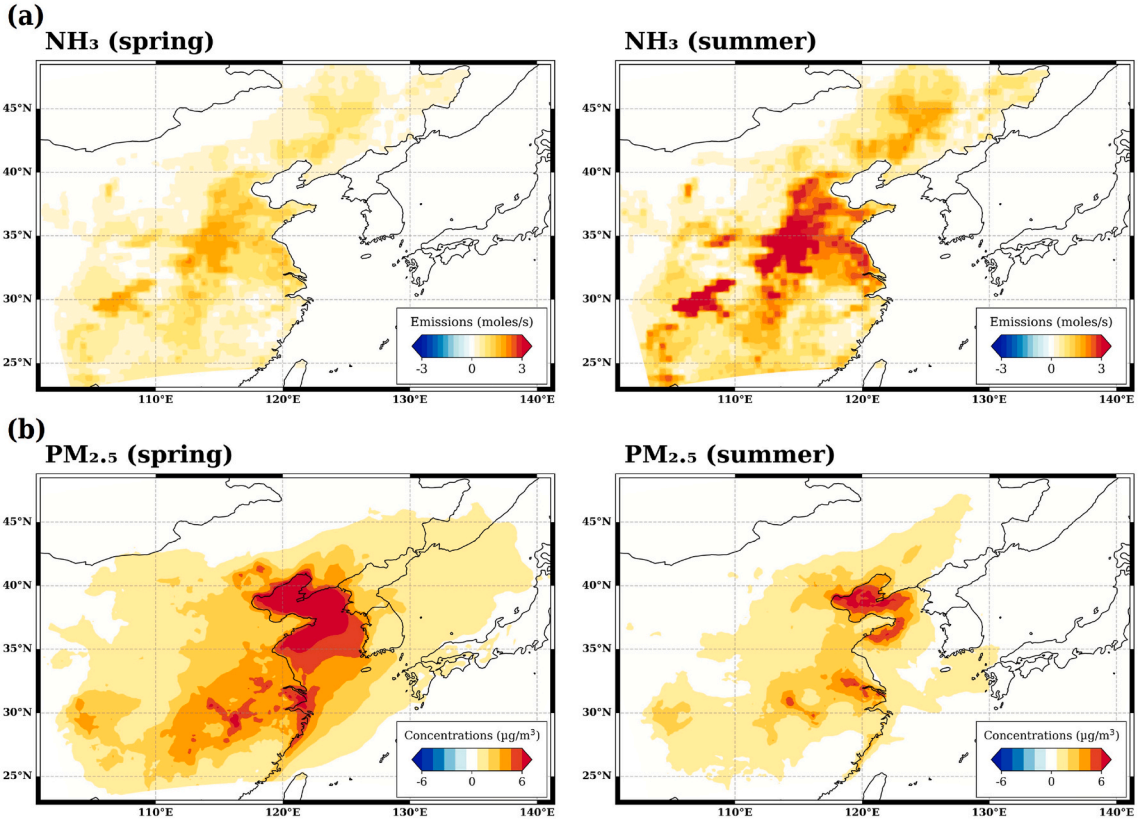

Fig. 3. Spatial distribution of seasonal mean differences (HIGH − BASE) in NH_3 emissions (a) and $PM_{2.5}$ concentrations (b) for spring and summer. All values represent averages at the surface layer.

concentrations predominate over ocean areas. Thus, the predominance of NO_3^- increases offshore indicates that the spatial distribution of HNO_3 was more important for NO_3^- formation.

Fig. 4, which illustrates the changes in HNO_3 and NO_3^- concentrations induced by increased NH_3 emissions in spring and summer, reveals that NO_3^- formation occurred predominantly over the ocean in both seasons. The marine atmosphere maintains lower temperatures and higher relative humidity compared to inland regions, thereby providing favorable conditions for NO_3^- formation (Seinfeld & Pandis, 2016; Hassan et al., 2013). In this study, increases in NH_3 emissions occurred primarily over inland regions, but local circulations and seasonal wind systems transported NH_3 to adjacent ocean areas. As a result, NO_3^- formation reactions also occurred offshore, explaining why these reactions were more pronounced over the ocean than inland. Especially in the Bohai Sea of northeastern China, NO_3^- concentrations increased by 6.11 $\mu g/m^3$ in spring and 3.53 $\mu g/m^3$ in summer, while HNO_3 decreased by 1.07 $\mu g/m^3$ in spring and 1.54 $\mu g/m^3$ in summer, both changes that exceed the domain averages. Surrounded on three sides by land, the Bohai Sea is geographically predisposed to receive elevated NH_3 fluxes from inland. Consequently, the combination of favorable marine atmospheric conditions and efficient NH_3 inflow amplified NO_3^- formation and HNO_3 depletion in this region. These findings suggest that regional circulation patterns and geographic configuration are key determinants of the spatial distribution of $PM_{2.5}$ component responses to emission increases.

Despite more pronounced NH_3 emissions and stronger HNO_3 depletion during summer, NO_3^- enhancements were larger in spring. This discrepancy implies that although the NO_3^- formation reaction consuming HNO_3 was more active during summer, additional NO_3^- removal may have occurred due to seasonal factors. Therefore, to quantify these seasonal differences in NO_3^- formation and loss, we applied the IPR tool in CMAQ to analyze NO_3^- concentration change rates separately over inland and ocean regions.

3.4. Seasonal mechanism analysis of NO_3^- formation and loss

Table 1 presents the changes in NO_3^- formation and removal rates for spring and summer as derived from the IPR analysis. In both seasons, NO_3^- formation over the ocean was strongly enhanced (spring +0.561 → summer +0.735 $\mu g/m^3/h$), whereas inland responses diverged. In spring, elevated NH_3 emissions induced additional NO_3^- production over land (+0.092 $\mu g/m^3/h$). In summer, however, the AERO process contribution of −1.454 $\mu g/m^3/h$ exceeded the total change rate of −1.229 $\mu g/m^3/h$, indicating dominant NO_3^- loss. To investigate why the AERO process exclusively caused NO_3^- loss in the summer inland, we conducted a vertical cross-section analysis.

Fig. 5 depicts the vertical cross-section of the NO_3^- concentration change rate (HIGH − BASE) driven by the AERO process. The analysis transect, defined from the western inland region to the eastern ocean area of the Bohai Sea (Fig. S16), was selected to account for NH_3 transport pathways along prevailing wind. Comparison of the spring and summer vertical cross-sections revealed that in summer over inland regions, NO_3^- loss was particularly pronounced, with this process concentrated in the lower PBL close to the surface (max: 3.71 $\mu g/m^3/h$).

Table 1
Season averaged rate of change in NO_3^- concentration ($\mu g/m^3/h$) attributed to individual physical and chemical processes, calculated by IPR analysis, averaged for values below the planetary boundary layer (PBL). The processes include horizontal transport (HT), vertical transport (VT), dry deposition (DDEP), and aerosol processes (AERO).

Season	Region	Total	HT	VT	DDEP	AERO
Spring	Ocean	0.561	−0.547	0.545	−0.114	0.677
	Inland	0.092	0.011	0.079	−0.120	0.121
Summer	Ocean	0.735	−0.741	0.872	−0.231	0.835
	Inland	−1.229	0.075	0.378	−0.228	−1.454

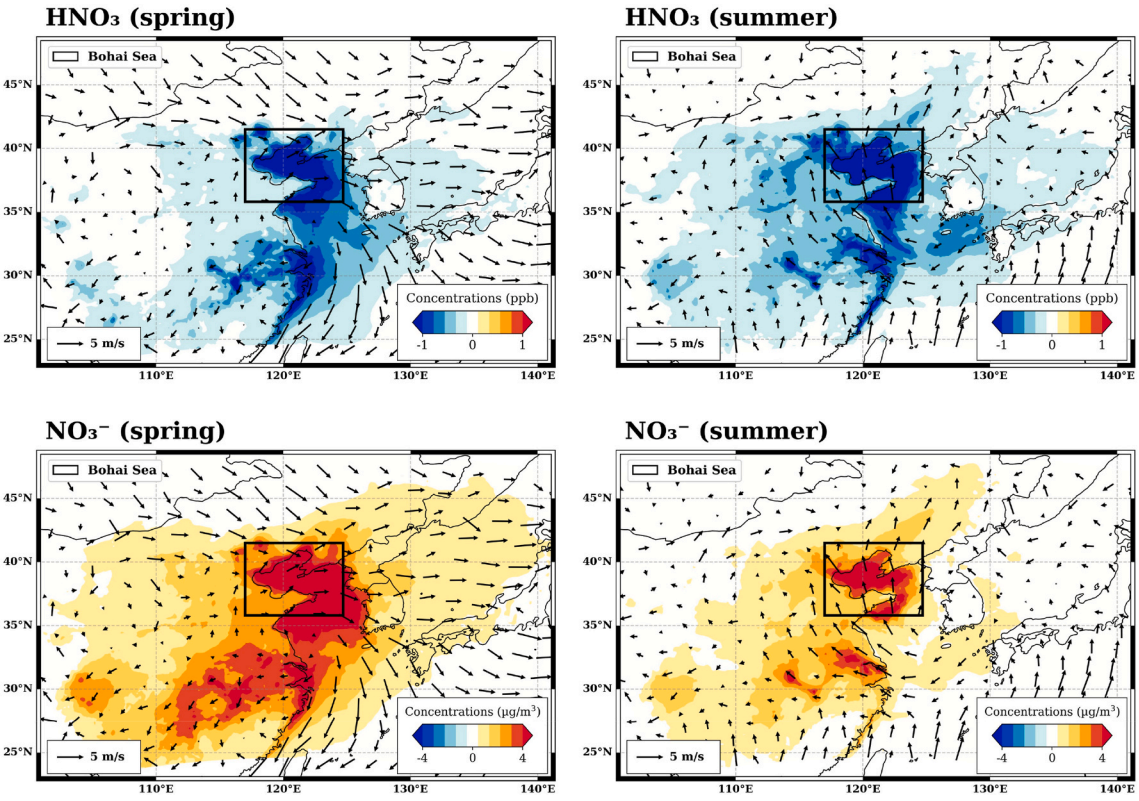

Fig. 4. Spatial distribution of seasonally averaged concentration differences (HIGH − BASE) of HNO_3 and NO_3^- for spring and summer. Black arrows indicate seasonally averaged surface wind vectors. The black box denotes the Bohai Sea region, where notable chemical responses occurred.

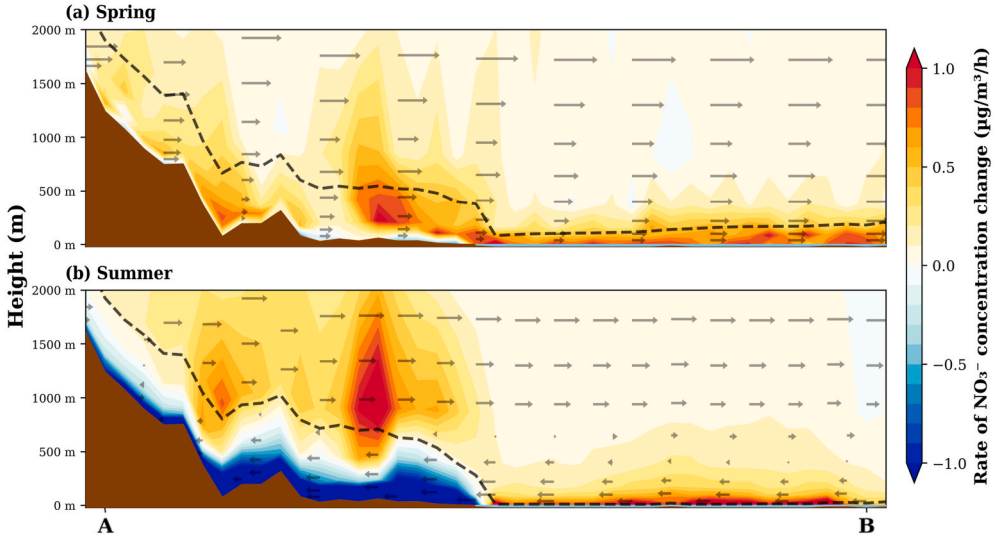

Fig. 5. Cross-sectional distribution of NO_3^- concentration change rates (μg/m^3/h) attributed to AERO processes for spring (a) and summer (b). Color shading indicates the rate of change in NO_3^- concentrations, and gray arrows represent the wind vectors along the cross-section. The black dashed line denotes the PBL height. (For interpretation of the references to colour in this figure legend, the reader is referred to the Web version of this article.)

This intensified surface layer loss is interpreted as resulting from increased chemical instability of NO_3^- at higher temperatures. Previous studies indicate that NO_3^- stability depends on temperature, humidity, and precursor concentrations, with dissociation of NH_4NO_3 into NH_3 and HNO_3 favored at higher temperatures (Seinfeld & Pandis, 2016; Saiz-Lopez et al., 2007). This behavior reflects the thermodynamic equilibrium of the NH_3–HNO_3–NH_4NO_3 system, which is explicitly represented in CMAQ through the ISORROPIA II module (Choi et al., 2025). According to Table S8, summer temperature increases relative to spring were far more pronounced inland (17.10 °C) than over the ocean (6.55 °C). Enhanced isolation during summer induced rapid inland warming, directly affecting NO_3^- stability. Consequently, increased dissociation of NO_3^- into HNO_3 and NH_3 occurred, manifesting as NO_3^- loss in the AERO process.

Seasonal variations in wind direction also exerted a pivotal influence on differences in NO_3^- production and loss. In spring, winds blowing from inland toward the ocean created favorable conditions for transporting NH_3 emitted over inland to ocean regions. However, the summer

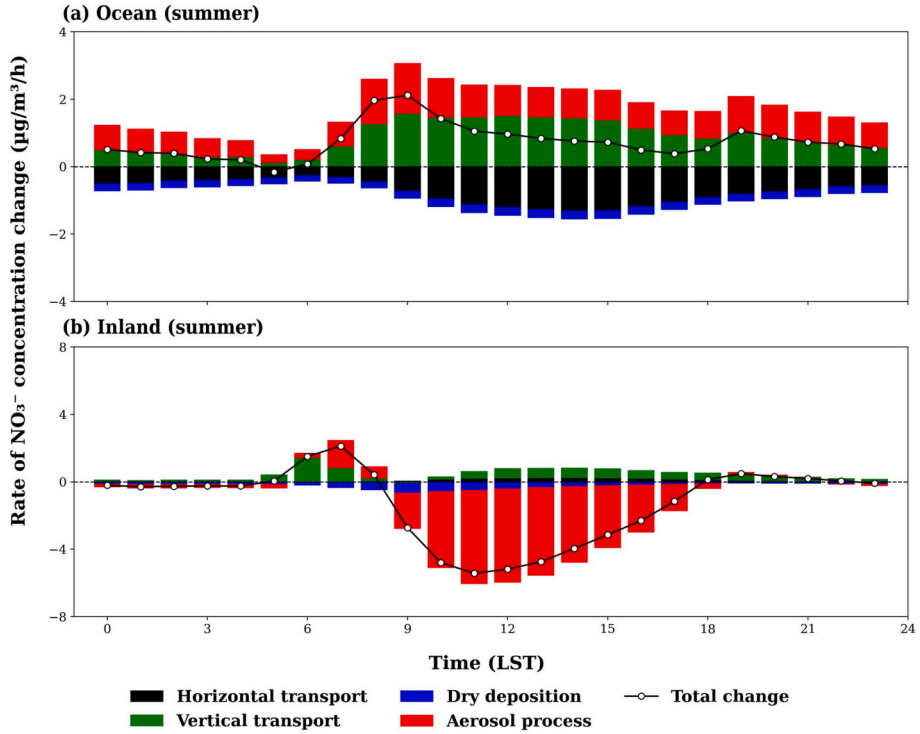

Fig. 6. Diurnal variation of NO_3^- concentration changes rates (μg/m^3/h) in summer based on IPR analysis. The top panel shows the oceanic region (a), and the down panel shows the inland region (b). Bars represent the contributions of individual processes in the HIGH − BASE case: horizontal transport (black), vertical transport (green), dry deposition (blue), and aerosol processes (red). The solid line with open circles indicates the total rate of change. (For interpretation of the references to colour in this figure legend, the reader is referred to the Web version of this article.)

winds primarily drove the onshore transport of NO_3^- already formed in the ocean, which subsequently destabilized and dissociated under the high inland temperatures. These findings are confirmed by the hourly IPR analysis for summer shown in Fig. 6. During summer over the ocean, the AERO process contributed +0.835 μg/m^3/h while horizontal transport removed −0.741 μg/m^3/h, indicating substantial export of NO_3^- formed over the ocean toward inland areas. NO_3^- exported from the ocean by horizontal transport was advected along the PBL top into upper layers and then subsided into the inland boundary layer via vertical transport. Accordingly, inland NO_3^- influx via vertical and horizontal transport amounted to +0.378 μg/m^3/h and +0.075 μg/m^3/h, respectively. This NO_3^- import served as the driver for enhanced NO_3^- loss by the AERO process during daytime inland.

Our IPR findings are broadly consistent with previous studies. For example, Sulaymon et al. (2023a) reported that emissions and aerosol processes dominated local $PM_{2.5}$ accumulation in the Beijing–Tianjin–Hebei region, with horizontal transport amplifying downwind pollution episodes. Similarly, Sun et al. (2022) demonstrated that in the Yangtze River Delta, daytime nitrate formation through the AERO process was strongly linked to HNO_3 production via the OH + NO_2 pathway, with faster formation rates under the warmer summer conditions. These studies support our interpretation that the increase in NO_3^- concentrations following enhanced NH_3 emissions is primarily driven by the AERO process.

Building on these insights, our results further reveal that the additionally formed NO_3^- is strongly influenced by seasonal meteorological conditions, which in turn drives the contrasting concentration responses between spring and summer. As illustrated in Fig. 7, NH_3 transported from inland to the ocean during spring enhanced NO_3^- production over the ocean, while relatively low temperatures contributed to the atmospheric stability of the newly formed NO_3^-. In summer, strong sunlight raised inland temperatures sharply and weakened NO_3^- stability. Summer winds then carried NO_3^- formed over the ocean back over land, where elevated temperatures accelerated their decomposition. These seasonal contrasts led to markedly lower NO_3^- concentration increases in summer compared to spring, identifying them as the key factors governing seasonal differences in $PM_{2.5}$ concentration responses.

4. Effects of seasonal wind on downwind $PM_{2.5}$ through long-range transport

Seasonal variations in atmospheric circulation and meteorological conditions were found to potentially influence changes in $PM_{2.5}$ concentrations over China. However, these emission changes affect not only local air quality near the sources but also $PM_{2.5}$ levels in downwind regions. As noted in the Introduction, seasonal shifts in wind patterns play a critical role in determining pollutant transport pathways and intensity. In South Korea, located to the east of China, these effects driven by wind can be even more pronounced than at the emission source. Therefore, in this section, we analyze $PM_{2.5}$ concentration changes in South Korea to evaluate how seasonal differences in prevailing wind influence the transport of pollutants into this downwind region.

Fig. 8 shows the horizontal distribution of $PM_{2.5}$ concentration changes induced by increased NH_3 emissions along the transect from the eastern inland of China to South Korea. In spring, as NH_3 emissions increased over inland China, $PM_{2.5}$ concentrations increased broadly across the Bohai Sea. Combined with prevailing westerly winds, this established a transport pathway reaching into inland South Korea. Consequently, springtime $PM_{2.5}$ concentrations over South Korea increased by an average of 2.12 μg/m^3, with maximum increases of 5.11 μg/m^3 along the west coast. In contrast, during summer, the concentration increases were confined to the Bohai Sea and the southern coastal waters off the Shandong Peninsula, and almost no transport to South Korea occurred. Accordingly, summer $PM_{2.5}$ concentration changes over South Korea increased by only 0.15 μg/m^3 on average, with a maximum increase of 0.70 μg/m^3.

These results demonstrate that seasonal variations in prevailing wind

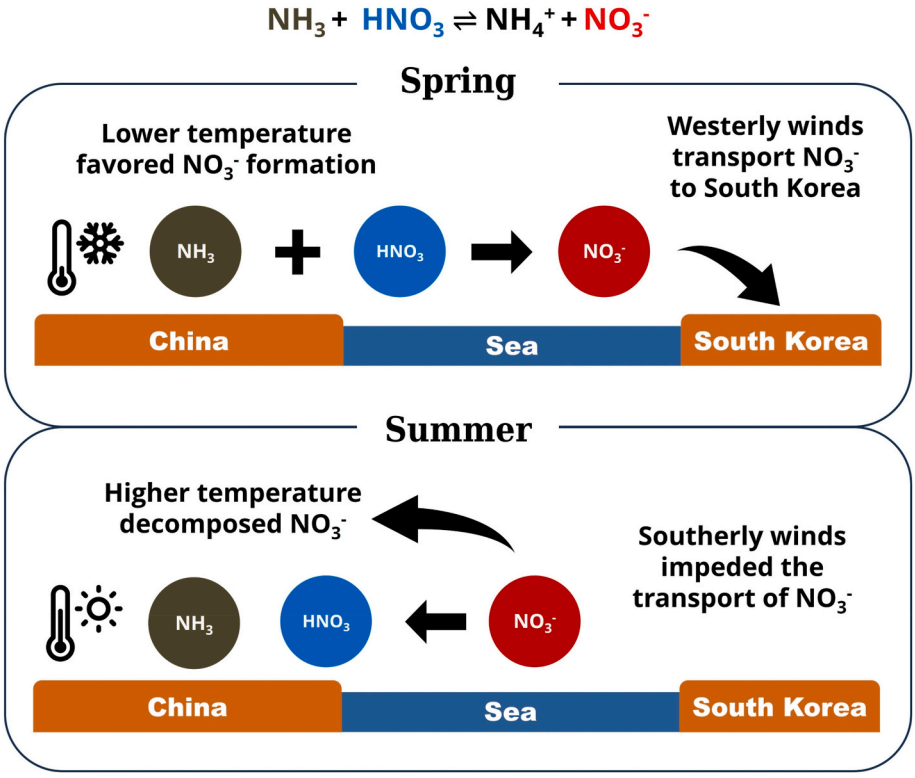

Fig. 7. Schematic illustration of seasonal mechanisms of NO_3^- formation and transport based on the thermodynamic equilibrium ($NH_3 + HNO_3 \rightleftharpoons NH_4^+ + NO_3^-$). The top panel shows spring conditions, and the bottom panel shows summer conditions.

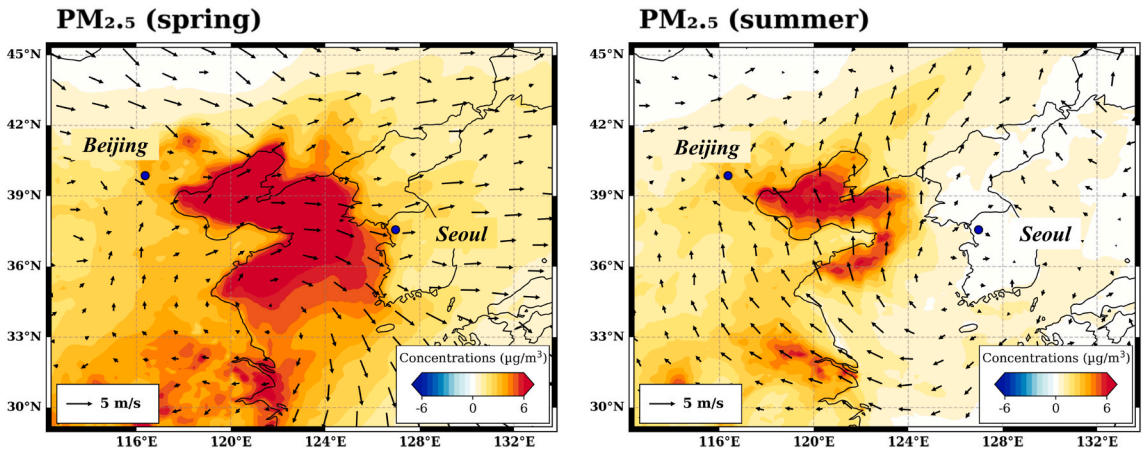

Fig. 8. Spatial distribution of $PM_{2.5}$ concentration differences (HIGH − BASE) and horizontal wind vectors for spring and summer. Blue dots mark the locations of Beijing, a representative upwind city, and Seoul, a representative downwind city located in South Korea. (For interpretation of the references to colour in this figure legend, the reader is referred to the Web version of this article.)

direction can directly influence the extent of air pollutant transport. In spring, predominant westerly winds efficiently carried pollutants from eastern China to western South Korea, whereas in summer, prevailing southerly winds weakened the transport pathway, leading to limited concentration increases in South Korea. To quantify these differences, we compared seasonal changes in $PM_{2.5}$ concentrations between the upwind region (Beijing) and the downwind region (Seoul) (Fig. S17). The analysis shows that Beijing's mean $PM_{2.5}$ increase was 2.75 μg/m^3 in spring and 2.42 μg/m^3 in summer, a seasonal difference of only 0.33 μg/m^3. In contrast, Seoul's increase was 3.07 μg/m^3 in spring versus 0.15 μg/m^3 in summer, yielding a seasonal difference of 2.92 μg/m^3. To further quantify transport efficiency, we calculated the ratio of concentration changes in Seoul to those in Beijing. The ratio was 1.12 in spring, indicating that the $PM_{2.5}$ response in the downwind region slightly exceeded that at the source, while in summer the ratio dropped to 0.06, reflecting minimal transport across the Yellow Sea. This simple metric highlights the stark seasonal contrast in transboundary transport and is consistent with approaches used in recent studies (Kim et al., 2024; Nirmalkar et al., 2024).The greater springtime increase in Seoul compared to its source region underscores that secondary pollutants like $PM_{2.5}$ can undergo amplification at downwind locations due to atmospheric chemistry and transport pathways.

This study highlights the significant influence of uncertainties in Chinese NH_3 emissions on $PM_{2.5}$ concentrations across East Asia, with impacts extending beyond the source region to downwind areas. Under East Asia's meteorological conditions, these effects may be particularly pronounced in spring. However, the distinct characteristics of autumn and winter, such as altered transport patterns, stagnant boundary layers, and reduced PBL heights, suggest that the responses of $PM_{2.5}$ to NH_3 emission changes may differ considerably across seasons, particularly as colder temperatures enhance the formation of NH_4NO_3 and can heighten $PM_{2.5}$ sensitivity to NH_3. In addition, this study relied on a single perturbation factor (+75.7 %) applied uniformly across China, which may not fully capture the spatial heterogeneity of actual emissions and thereby introduces additional uncertainty. Future studies should therefore explore regionally weighted sensitivity experiments and incorporate alternative emission inventories such as MEIC to strengthen the robustness of the findings. Furthermore, this study did not include natural emission sources such as sea salt and dust. As the interactions between these natural aerosols and anthropogenic pollutants can alter $PM_{2.5}$ formation pathways, their inclusion is necessary in future studies for a more comprehensive analysis.

Despite these limitations, the results of this study underscore that the underestimation of NH_3 emissions can lead models to overstate the effectiveness of emission reduction strategies, carrying direct implications for both air quality management and health impact assessments. Addressing these uncertainties through more comprehensive approaches will not only improve the reliability of NH_3 simulations but also enhance the accuracy of air quality forecasts and health burden evaluations across East Asia, ultimately supporting the design of more effective pollution control policies.

5. Conclusions

In this study, we used the CMAQ model to evaluate the impacts of uncertainties in Chinese NH_3 emissions on air quality in China and South Korea. The analysis focused on spring and summer 2019 by comparing a baseline scenario with an enhanced emission scenario. Increased NH_3 emissions elevated $PM_{2.5}$ concentrations in both China and South Korea, with mean increases of 2.54 μg/m^3 in spring and 1.99 μg/m^3 in summer, and the largest enhancement was observed in NO_3^- produced via the NH_3–HNO_3 reaction. Strikingly, despite stronger NO_3^- production and HNO_3 consumption in summer, the net increase in NO_3^- concentrations was higher in spring. To resolve this apparent contradiction, we applied the IPR analysis to track NO_3^- formation and loss, which revealed that enhanced NO_3^- loss through the AERO process offset production in summer. In both seasons, additional NO_3^- formation due to increased NH_3 emissions occurred mainly over marine regions such as the Bohai Sea, highlighting the critical role of HNO_3 availability in driving NO_3^- production. However, seasonal wind patterns modulated the transport and fate of NO_3^-. In spring, prevailing westerly winds facilitated the export of newly formed NO_3^- from inland regions toward the ocean. In summer, by contrast, southerly winds transported NO_3^- formed over the ocean back inland, where elevated temperatures favored its decomposition into NH_3 and HNO_3. This process suppressed the rise in $PM_{2.5}$ concentrations. These seasonal environmental contrasts influenced not only the mechanisms of NO_3^- formation over inland and oceanic regions of China but also the resulting $PM_{2.5}$ concentration changes in downwind South Korea. In particular, the $PM_{2.5}$ increase in Seoul during spring reached 3.07 μg/m^3, exceeding the 2.75 μg/m^3 increase observed in Beijing, whereas in summer the increase in Seoul was only 0.15 μg/m^3, much lower than the 2.42 μg/m^3 observed in Beijing, highlighting the more pronounced seasonal disparity in the downwind region.

CRediT authorship contribution statement

Hyeonsik Choe: Writing – original draft, Investigation, Conceptualization. **Chae-Yeong Yang:** Visualization, Data curation. **Yunsoo Choi:** Writing – review & editing, Supervision. **Jincheol Park:** Methodology, Investigation. **Dongjin Kim:** Writing – review & editing.

Jeonghyeok Moon: Software, Methodology. **Min Heo:** Software, Methodology. **Jaehyeong Park:** Validation. **Cheol-Hee Kim:** Project administration, Funding acquisition. **Wonbae Jeon:** Writing – review & editing, Supervision, Conceptualization.

Declaration of competing interest

The authors declare that they have no known competing financial interests or personal relationships that could have appeared to influence the work reported in this paper.

Acknowledgments

This research was partially supported by Korea Environmental Industry & Technology Institute (KEITI) through "Project for developing an observation-based GHG emissions geospatial information map", funded by Korea Ministry of Environment (MOE) (RS-2023-00232066) and the Basic Science Research Program through the National Research Foundation of Korea (NRF) funded by the Ministry of Education (RS-2020-NR049592).

Appendix A. Supplementary data

Supplementary data to this article can be found online at https://doi.org/10.1016/j.envpol.2025.127159.

Data availability

Data will be made available on request.

References

Appel, K.W., Bash, J.O., Fahey, K.M., Foley, K.M., Gilliam, R.C., Hogrefe, C., Hutzell, W. T., Kang, D., Mathur, R., Murphy, B.N., 2021. The community Multiscale air quality (CMAQ) model versions 5.3 and 5.3.1: system updates and evaluation. Geosci. Model Dev. (GMD) 14 (5), 2867–2897. https://doi.org/10.5194/gmd-14-2867-2021.

Bae, C., Kim, B.U., Kim, H.C., Yoo, C., Kim, S., 2019. Long-range transport influence on key chemical components of $PM_{2.5}$ in the Seoul metropolitan area, South Korea, during the years 2012–2016. Atmosphere 11 (1), 48. https://doi.org/10.3390/atmos11010048.

Bell, M.L., Dominici, F., Ebisu, K., Zeger, S.L., Samet, J.M., 2007. Spatial and temporal variation in $PM_{2.5}$ chemical composition in the United States for health effects studies. Environ. Health Perspect. 115 (7), 989–995. https://doi.org/10.1289/ehp.9621.

Boylan, J.W., Russell, A.G., 2006. PM and light extinction model performance metrics, goals, and criteria for three-dimensional air quality models. Atmos. Environ. 40 (26), 4946–4959. https://doi.org/10.1016/j.atmosenv.2005.09.087.

Byon, J.-Y., Choi, Y.-J., Seo, B.-K., 2010. Characteristics of a wind map over the Korean Peninsula based on mesoscale model WRF. Atmosphere 20 (2), 195–210. https://koreascience.kr/article/JAKO201028839764899.pdf.

Cao, Z., Zhou, X., Ma, Y., Wang, L., Wu, R., Chen, B., Wang, W., 2017. The concentrations, formations, relationships and modeling of sulfate, nitrate and ammonium aerosols over China. Aerosol Air Qual. Res. 17 (1), 84–97. https://doi.org/10.4209/aaqr.2016.01.0020.

Chen, J., Cheng, M., Krol, M., de Vries, W., Zhu, Q., Liu, X., Zhang, F., Xu, W., 2023. Trends in anthropogenic ammonia emissions in China since 1980: a review of approaches and estimations. Front. Environ. Sci. 11, 1133753. https://doi.org/10.3389/fenvs.2023.1133753.

Cheng, Z., Luo, L., Wang, S., Wang, Y., Sharma, S., Shimadera, H., Wang, X., Bressi, M., de Miranda, R.M., Jiang, J., 2016. Status and characteristics of ambient $PM_{2.5}$ pollution in global megacities. Environ. Int. 89, 212–221. https://doi.org/10.1016/j.envint.2016.02.003.

Ching, J., Byun, D., 1999. Introduction to the Models-3 framework and the community multiscale Air Quality model (CMAQ). Sci. Algorithms EPA Models-3 Community Multiscale Air Quality (CMAQ) Modeling Syst., 20460. https://api.semanticscholar.org/CorpusID:31614643.

Choi, J., Nirmalkar, J., Lee, K., Song, M., 2025. Reducing particulate NO3− of PM2.5 under an ammonia-rich environment: role of NH_3 and aerosol pH using ISORROPIA-II model. Atmos. Environ. 343, 120988. https://doi.org/10.1016/j.atmosenv.2024.120988.

Choi, S.-w., Cho, H., Hong, Y., Jo, H.-j., Park, M., Lee, H.-j., Choi, Y.-j., Shin, H.-h., Lee, D., Shin, E., 2022. Analysis of the National Air pollutant Emissions Inventory (CAPSS 2018) data and assessment of emissions based on air quality modeling in the Republic of Korea. Asian J. Atmos. Environ. 16 (4), 2022084. https://doi.org/10.5572/ajae.2022.084.

Clarisse, L., Clerbaux, C., Dentener, F., Hurtmans, D., Coheur, P.F., 2009. Global ammonia distribution derived from infrared satellite observations. Nat. Geosci. 2 (7), 479–483. https://doi.org/10.1038/ngeo551.

Clarisse, L., Franco, B., Van Damme, M., Di Gioacchino, T., Hadji-Lazaro, J., Whitburn, S., Noppen, L., Hurtmans, D., Clerbaux, C., Coheur, P., 2023. The IASI NH_3 version 4 product: averaging kernels and improved consistency. Atmos. Meas. Tech. 16, 5009–5039. https://doi.org/10.5194/amt-16-5009-2023.

Crippa, M., Guizzardi, D., Butler, T., Keating, T., Wu, R., Kaminski, J., Kuenen, J., Kurokawa, J., Chatani, S., Morikawa, T., 2023. The HTAP_v3 emission mosaic: merging regional and global monthly emissions (2000–2018) to support air quality modelling and policies. Earth Syst. Sci. Data 15 (6), 2667–2694. https://doi.org/10.5194/essd-15-2667-2023.

Damme, M., Whitburn, S., Clarisse, L., Clerbaux, C., Hurtmans, D., Coheur, P., 2017. Version 2 of the IASI NH_3 neural network retrieval algorithm: near-real-time and reanalysed datasets. Atmos. Meas. Tech. 10 (12), 4905–4914. https://doi.org/10.5194/amt-10-4905-2017.

Dong, W., Xing, J., Wang, S., 2010. Temporal and spatial distribution of anthropogenic ammonia emissions in China: 1994–2006. Huanjing Kexue 31 (7), 1457–1463. https://doi.org/10.13227/j.hjkx.2010.07.008.

Emery, C., Jung, J., Koo, B., Yarwood, G., 2015. Improvements to CAMx snow cover treatments and Carbon Bond chemical mechanism for winter ozone. Final Rep 535. https://www.camx.com/files/udaq_snowchem_final_6aug15.pdf.

Emery, C., Liu, Z., Russell, A.G., Odman, M.T., Yarwood, G., Kumar, N., 2017. Recommendations on statistics and benchmarks to assess photochemical model performance. J. Air Waste Manag. Assoc. 67 (5), 582–598. https://doi.org/10.1080/10962247.2016.1265027.

Erisman, J., Schaap, M., 2004. The need for ammonia abatement with respect to secondary PM reductions in Europe. Environ. Pollut. 129 (1), 159–163. https://doi.org/10.1016/j.envpol.2003.08.042.

Fountoukis, C., Nenes, A., 2007. Isorropia II: a computationally efficient thermodynamic equilibrium model for K^+–Ca^{2+}–Mg^{2+}–NH^{4+}–Na^+–SO_4^{2-}–NO_3^-–Cl^-–H_2O aerosols. Atmos. Chem. Phys. 7 (17), 4639–4659. https://doi.org/10.5194/acp-7-4639-2007.

Franco, B., Clarisse, L., Stavrakou, T., Müller, J.F., Van Damme, M., Whitburn, S., Hadji-Lazaro, J., Hurtmans, D., Taraborrelli, D., Clerbaux, C., 2018. A general framework for global retrievals of trace gases from IASI: application to methanol, formic acid, and PAN. J. Geophys. Res. Atmos. 123 (24), 13963–13984. https://doi.org/10.1029/2018JD029633.

Gong, Y., Zhou, H., Chun, X., Wan, Z., Wang, J., Liu, C., 2024. Response of $PM_{2.5}$ chemical composition to the emission reduction and meteorological variation during the COVID-19 lockdown. Chemosphere 363, 142844. https://doi.org/10.1016/j.chemosphere.2024.142844.

Guenther, A., Jiang, X., Heald, C.L., Sakulyanontvittaya, T., Duhl, T., Emmons, L., Wang, X., 2012. The Model of emissions of gases and Aerosols from nature version 2.1 (MEGAN2.1): an extended and updated framework for modeling biogenic emissions. Geosci. Model Dev. (GMD) 5 (6), 1471–1492. https://doi.org/10.5194/gmd-5-1471-2012.

Hassan, S.K., El-Abssawy, A.A., Khoder, M.I., 2013. Characteristics of gas-phase nitric acid and ammonium-nitrate-sulfate aerosol, and their gas-phase precursors in a suburban area in Cairo, Egypt. Atmos. Pollut. Res. 4 (1), 117–129. https://doi.org/10.5094/APR.2013.012.

Hersbach, H., Bell, B., Berrisford, P., Hirahara, S., Horányi, A., Muñoz-Sabater, J., Nicolas, J., Peubey, C., Radu, R., Schepers, D., 2020. The ERA5 global reanalysis. Q. J. R. Meteorol. Soc. 146 (730), 1999–2049. https://doi.org/10.1002/qj.3803.

Hua, J., Zhang, Y., Chen, J., Shang, Y., Hu, X., de Foy, B., Sulaymon, I.D., Zhang, Y., Wu, Z., 2024. Unravelling the impacts of stratospheric intrusions on near-surface ozone during the springtime ozone pollution episodes in Lhasa, China. Atmos. Res. 311, 107687. https://doi.org/10.1016/j.atmosres.2024.107687.

Huang, X., Song, Y., Li, M., Li, J., Huo, Q., Cai, X., Zhu, T., Hu, M., Zhang, H., 2012. A high-resolution ammonia emission inventory in China. Glob. Biogeochem. Cycles 26 (1). https://doi.org/10.1029/2011GB004161.

Jeon, W., Choi, Y., Lee, H.W., Lee, S.H., Yoo, J.W., Park, J., Lee, H.J., 2015. A quantitative analysis of grid nudging effect on each process of $PM_{2.5}$ production in the Korean Peninsula. Atmos. Environ. 122, 763–774. https://doi.org/10.1016/j.atmosenv.2015.10.050.

Jeon, W., Park, J., Choi, Y., Mun, J., Kim, D., Kim, C.H., Lee, H.J., Bak, J., Jo, H.Y., 2021. The mechanism of the formation of high sulfate concentrations over the Yellow Sea during the KORUS-AQ period: the effect of transport/atmospheric chemistry and ocean emissions. Atmos. Res. 261, 105756. https://doi.org/10.1016/j.atmosres.2021.105756.

Kai, Z., Yuesi, W., Tianxue, W., Yousef, M., Frank, M., 2007. Properties of nitrate, sulfate and ammonium in typical polluted atmospheric aerosols (PM_{10}) in Beijing. Atmos. Res. 84 (1), 67–77. https://doi.org/10.1016/j.atmosres.2006.05.004.

Kaneyasu, N., Yamamoto, S., Sato, K., Takami, A., Hayashi, M., Hara, K., Kawamoto, K., Okuda, T., Hatakeyama, S., 2014. Impact of long-range transport of aerosols on the $PM_{2.5}$ composition at a major metropolitan area in the northern Kyushu area of Japan. Atmos. Environ. 97, 416–425. https://doi.org/10.1016/j.atmosenv.2014.01.029.

Kharol, S., Martin, R., Philip, S., Vogel, S., Henze, D., Chen, D., Wang, Y., Zhang, Q., Heald, C., 2013. Persistent sensitivity of Asian aerosol to emissions of nitrogen oxides. Geophys. Res. Lett. 40 (5), 1021–1026. https://doi.org/10.1002/grl.50234.

Kim, B.U., Bae, C., Kim, H.C., Kim, E., Kim, S., 2017a. Spatially and chemically resolved source apportionment analysis: case study of high particulate matter event. Atmos. Environ. 162, 55–70. https://doi.org/10.1016/j.atmosenv.2017.05.006.

Kim, D., Choi, Y., Jeon, W., Mun, J., Park, J., Kim, C.H., Yoo, J.W., 2024. Quantitative analysis of sulfate formation from crop burning in Northeast China: unveiling the

primary processes and transboundary transport to South Korea. Atmos. Res. 302, 107303. https://doi.org/10.1016/j.atmosres.2024.107303.
Kim, H.C., Kim, E., Bae, C., Cho, J.H., Kim, B.U., Kim, S., 2017b. Regional contributions to particulate matter concentration in the Seoul metropolitan area, South Korea: seasonal variation and sensitivity to meteorology and emissions inventory. Atmos. Chem. Phys. 17 (17), 10315–10332. https://doi.org/10.5194/acp-17-10315-2017.
Kurokawa, J., Ohara, T., 2019. Long-term historical trends in air pollutant emissions in Asia: regional Emission inventory in ASia (REAS) version 3.1. Atmos. Chem. Phys. 20, 12761–12793. https://doi.org/10.5194/acp-20-12761-2020.
Li, L., Huang, C., Huang, H., Wang, Y., Yan, R., Zhang, G., Zhou, M., Lou, S., Tao, S., Wang, H., 2014. An integrated process rate analysis of a regional fine particulate matter episode over the Yangtze River Delta in 2010. Atmos. Environ. 91, 60–70. https://doi.org/10.1016/j.atmosenv.2014.03.053.
Liang, Y., Jiang, H., Liu, X., 2024. Characteristics of atmospheric ammonia and its impacts on SNA formation in $PM_{2.5}$ of Nanchang. China. Atmos. Pollut. Res. 15 (4), 102059. https://doi.org/10.1016/j.apr.2024.102059.
Lim, K.-S.S., Lim, J.-M., Shin, H.H., Hong, J., Ji, Y.-Y., Lee, W., 2019. Impacts of subgrid-scale orography parameterization on simulated atmospheric fields over Korea using a high-resolution atmospheric forecast model. Meteorol. Atmos. Phys. 131 (4), 975–985. https://doi.org/10.1007/s00703-018-0615-4.
Liu, H.Y., Dunea, D., Iordache, S., Pohoata, A., 2018. A review of airborne particulate matter effects on young children's respiratory symptoms and diseases. Atmosphere 9 (4), 150. https://doi.org/10.3390/atmos9040150.
Liu, P., Ding, J., Liu, L., Xu, W., Liu, X., 2022. Estimation of surface ammonia concentrations and emissions in China from the polar-orbiting Infrared Atmospheric sounding interferometer and the FY-4A Geostationary interferometric Infrared sounder. Atmos. Chem. Phys. 22 (13), 9099–9110. https://doi.org/10.5194/acp-22-9099-2022.
Liu, X.H., Zhang, Y., Xing, J., Zhang, Q., Wang, K., Streets, D.G., Jang, C., Wang, W.X., Hao, J.M., 2010. Understanding of regional air pollution over China using CMAQ, part II. Process analysis and sensitivity of ozone and particulate matter to precursor emissions. Atmos. Environ. 44 (30), 3719–3727. https://doi.org/10.1016/j.atmosenv.2010.03.036.
Liu, X., Xu, W., Du, E., Tang, A., Zhang, Y., Zhang, Y., Wen, Z., Hao, T., Pan, Y., Zhang, L., 2020. Environmental impacts of nitrogen emissions in China and the role of policies in emission reduction. Philos. Trans. R. Soc. A 378 (2183), 20190324. https://doi.org/10.1098/rsta.2019.0324.
Mao, J., Li, L., Li, J., Sulaymon, I.D., Xiong, K., Wang, K., Zhu, J., Chen, G., Ye, F., Zhang, N., 2022. Evaluation of long-term modeling fine particulate matter and ozone in China during 2013–2019. Front. Environ. Sci. 10, 872249. https://doi.org/10.3389/fenvs.2022.872249.
Mathur, R., Xing, J., Gilliam, R., Sarwar, G., Hogrefe, C., Pleim, J., Pouliot, G., Roselle, S., Spero, T.L., Wong, D.C., 2017. Extending the community multiscale Air Quality (CMAQ) modeling system to hemispheric scales: overview of process considerations and initial applications. Atmos. Chem. Phys. 17 (20), 12449–12474. https://doi.org/10.5194/acp-17-12449-2017.
Momeni, M., Choi, Y., Yeganeh, A.K., Pouyaei, A., Jung, J., Park, J., Shephard, M.W., Dammers, E., Cady-Pereira, K.E., 2024. Constraining East Asia ammonia emissions through satellite observations and iterative Finite difference Mass Balance (iFDMB) and investigating its impact on inorganic fine particulate matter. Environ. Int. 184, 108473. https://doi.org/10.1016/j.envint.2024.108473.
Nirmalkar, J., Haswani, D., Singh, A., Kumar, S., Raman, R.S., 2021. Concentrations, transport characteristics, and health risks of $PM_{2.5}$-bound trace elements over a national park in central India. J. Environ. Manage. 293, 112904. https://doi.org/10.1016/j.jenvman.2021.112904.
Nirmalkar, J., Jung, J., Han, S., Dong, Z., Xu, Z., Fu, P., Pavulari, C.M., 2023. Chemistry of $PM_{2.5}$ in haze events in two East Asian cities during winter–spring 2019. Atmos. Environ. 293, 119457. https://doi.org/10.1016/j.atmosenv.2022.119457.
Nirmalkar, J., Lee, J.Y., Lee, K., Ahn, J., Qiu, Y., Wu, Z., Natsagdorj, A., Jang, K.-S., Kim, C., Song, M., 2024. Impact of biomass burning on $PM_{2.5}$ and organic aerosol: quantitative estimates and spatial distributions in four Northeast Asian sites. Atmos. Environ. 333, 120635. https://doi.org/10.1016/j.atmosenv.2024.120635.
Oh, H.R., Ho, C.H., Kim, J., Chen, D., Lee, S., Choi, Y.S., Chang, L.S., Song, C.K., 2015. Long-range transport of air pollutants originating in China: a possible major cause of multi-day high-PM_{10} episodes during cold season in Seoul, Korea. Atmos. Environ. 109, 23–30. https://doi.org/10.1016/j.atmosenv.2015.03.005.
Park, J., Jung, J., Choi, Y., Mousavinezhad, S., Pouyaei, A., 2022. The sensitivities of ozone and $PM_{2.5}$ concentrations to the satellite-derived leaf area index over East Asia and its neighboring seas in the WRF-CMAQ modeling system. Environ. Pollut. 306, 119419. https://doi.org/10.1016/j.envpol.2022.119419.
Park, J., Jung, J., Choi, Y., Lim, H., Kim, M., Lee, K., Lee, Y.G., Kim, J., 2023. Satellite-based, top-down approach for the adjustment of aerosol precursor emissions over East Asia: the TROPOspheric monitoring Instrument (TROPOMI) NO_2 product and the Geostationary Environment Monitoring Spectrometer (GEMS) aerosol optical depth (AOD) data fusion product and its proxy. Atmos. Meas. Tech. 16 (12), 3039–3057. https://doi.org/10.5194/amt-16-3039-2023.
Park, J., Choi, Y., Kayastha, S., 2025. Local and transboundary contributions to NO_y loadings across East Asia using CMAQ-ISAM and a GEMS-informed emission inventory during the winter–spring transition. Atmos. Chem. Phys. 25 (7), 4291–4311. https://doi.org/10.5194/acp-25-4291-2025.
Pun, V.C., Kazemiparkouhi, F., Manjourides, J., Suh, H.H., 2017. Long-term $PM_{2.5}$ exposure and respiratory, cancer, and cardiovascular mortality in older US adults. Am. J. Epidemiol. 186 (8), 961–969. https://doi.org/10.1093/aje/kwx166.
Qu, K., Wang, X., Xiao, T., Shen, J., Lin, T., Chen, D., He, L.Y., Huang, X.F., Zeng, L., Lu, K., 2021. Cross-regional transport of $PM_{2.5}$ nitrate in the Pearl River Delta, China: contributions and mechanisms. Sci. Total Environ. 753, 142439. https://doi.org/10.1016/j.scitotenv.2020.142439.
Saiz-Lopez, A., Notario, A., Albaladejo, J., McFiggans, G., 2007. Seasonal variation of NO_x loss processes coupled to the HNO3 formation in a daytime urban atmosphere: a model study. Water Air Soil Pollut. 182, 197–206. https://doi.org/10.1007/s11270-006-9332-6.
Seinfeld, J.H., Pandis, S.N., 2016. Atmospheric Chemistry and Physics: from Air Pollution to Climate Change, third ed. John Wiley & Sons, Hoboken, NJ. https://doi.org/10.1007/s00703-018-00033-5.
Shen, J., Zhao, Q., Cheng, Z., Wang, P., Ying, Q., Liu, J., Duan, Y., Fu, Q., 2020. Insights into source origins and formation mechanisms of nitrate during winter haze episodes in the Yangtze River Delta. Sci. Total Environ. 741, 140187. https://doi.org/10.1016/j.scitotenv.2020.140187.
Skamarock, W.C., Klemp, J.B., Dudhia, J., Gill, D.O., Liu, Z., Berner, J., Wang, W., Powers, J.G., Duda, M.G., Barker, D.M., 2019. A description of the advanced research WRF model version 4. NCAR Tech. Note NCAR/TN-556+STR 145. https://www2.mmm.ucar.edu/wrf/users/docs/technote/v4_technote.pdf.
Souri, A.H., Choi, Y., Jeon, W., Woo, J.H., Zhang, Q., Kurokawa, J.i., 2017. Remote sensing evidence of decadal changes in major tropospheric ozone precursors over East Asia. J. Geophys. Res. Atmos. 122 (4), 2474–2492. https://doi.org/10.1002/2016JD025663.
Sulaymon, I.D., Zhang, Y., Hopke, P.K., Ye, F., Gong, K., Mao, J., Hu, J., 2023a. Modeling $PM_{2.5}$ during severe atmospheric pollution episode in Lagos, Nigeria: spatiotemporal variations, source apportionment, and meteorological influences. J. Geophys. Res. Atmos. 128, e2022JD038360. https://doi.org/10.1029/2022JD038360.
Sulaymon, I.D., Zhang, Y., Hopke, P.K., Guo, S., Ye, F., Sun, J., Zhu, Y., Hu, J., 2023b. Using the COVID-19 lockdown to identify atmospheric processes and meteorology influences on regional $PM_{2.5}$ pollution episodes in the Beijing-Tianjin-Hebei, China. Atmos. Res. 294, 106940. https://doi.org/10.1016/j.atmosres.2023.106940.
Sun, J., Qin, M., Xie, X., Fu, W., Qin, Y., Sheng, L., Li, L., Li, J., Sulaymon, I.D., Jiang, L., 2022. Seasonal modeling analysis of nitrate formation pathways in Yangtze River Delta region, China. Atmos. Chem. Phys. 22 (18), 12629–12646. https://doi.org/10.5194/acp-22-12629-2022.
U.S. Environmental Protection Agency (EPA), 2018. Seasonal average hemispheric CMAQ output for 2016 (CCTM_CONC_v53beta2_intel17.0_HEMIS_cb6r3m_ae7_kmtbr_m3dry_2016_quarterly_av.nc). CMAS Data Warehouse. https://drive.google.com/file/d/15Vt6f5WuyN8RiLRjTlKeQUHjYbZ6QCrA. (Accessed 18 June 2025).
Van Damme, M., Clarisse, L., Heald, C.L., Hurtmans, D., Ngadi, Y., Clerbaux, C., Dolman, A., Erisman, J.W., Coheur, P.F., 2014. Global distributions, time series and error characterization of atmospheric ammonia (NH_3) from IASI satellite observations. Atmos. Chem. Phys. 14 (6), 2905–2922. https://doi.org/10.5194/acp-14-2905-2014.
Van Damme, M., Erisman, J.W., Clarisse, L., Dammers, E., Whitburn, S., Clerbaux, C., Dolman, A.J., Coheur, P.F., 2015. Worldwide spatiotemporal atmospheric ammonia (NH_3) columns variability revealed by satellite. Geophys. Res. Lett. 42 (20), 8660–8668. https://doi.org/10.1002/2015GL065496.
Wang, L., Chen, X., Zhang, Y., Li, M., Li, P., Jiang, L., Xia, Y., Li, Z., Li, J., Wang, L., 2021. Switching to electric vehicles can lead to significant reductions of $PM_{2.5}$ and NO_2 across China. One Earth 4 (7), 1037–1048. https://doi.org/10.1016/j.oneear.2021.06.008.
Wang, X., Li, L., Gong, K., Mao, J., Hu, J., Li, J., Liu, Z., Liao, H., Qiu, W., Yu, Y., 2021. Modelling air quality during the EXPLORE-YRD campaign – part I. Model performance evaluation and impacts of meteorological inputs and grid resolutions. Atmos. Environ. 246, 118131. https://doi.org/10.1016/j.atmosenv.2020.118131.
Wang, S., Zhang, M., Gao, Y., Wang, P., Fu, Q., Zhang, H., 2024. Diagnosing drivers of PM2.5 simulation biases in China from meteorology, chemical composition, and emission sources using an efficient machine learning method. Geosci. Model Dev. (GMD) 17 (9), 3617–3629. https://doi.org/10.5194/gmd-17-3617-2024.
Ye, B., Ji, X., Yang, H., Yao, X., Chan, C.K., Cadle, S.H., Chan, T., Mulawa, P.A., 2003. Concentration and chemical composition of $PM_{2.5}$ in Shanghai for a 1-year period. Atmos. Environ. 37 (4), 499–510. https://doi.org/10.1016/S1352-2310(02)00918-4.
Ye, F., Rupakheti, D., Huang, L., Mk, S.K., Li, L., Kt, V., Hu, J., 2022. Integrated process analysis retrieval of changes in ground-level ozone and fine particulate matter during the COVID-19 outbreak in the coastal city of Kannur, India. Environ. Pollut. 307, 119468. https://doi.org/10.1016/j.envpol.2022.119468.
Zhan, Y., Xie, M., Zhao, W., Wang, T., Gao, D., Chen, P., Tian, J., Zhu, K., Li, S., Zhuang, B., 2023. Quantifying the seasonal variations in and regional transport of $PM_{2.5}$ in the Yangtze River Delta region, China: characteristics, sources, and health risks. Atmos. Chem. Phys. 23 (17), 9837–9852. https://doi.org/10.5194/acp-23-9837-2023.
Zheng, B., Tong, D., Li, M., Liu, F., Hong, C., Geng, G., Li, H., Li, X., Peng, L., Qi, J., 2018. Trends in China's anthropogenic emissions since 2010 as the consequence of clean air actions. Atmos. Chem. Phys. 18 (19), 14095–14111. https://doi.org/10.5194/acp-18-14095-2018.